Aseismic creep along the San Andreas Fault northwest of Parkfield, CA measured by radar interferometry

P. Rosen, C. Werner, E. Fielding, S. Hensley, S. Buckley[†], P. Vincent[*]

Jet Propulsion Laboratory, Pasadena, California

[†] Center for Space Research, The University of Texas at Austin

[*] University of Colorado, Boulder, Colorado

Abstract.
ERS-1 radar images acquired 14 months apart studied by differential radar interferometry show the wide-area distribution of aseismic creep along the fault segment northwest of Parkfield, California. A sharp discontinuity in the interferometric phase of less than 2 cm equivalent line-of-sight displacement extends over 80 km in the differential interferogram, coincident with the mapped trace of the active San Andreas fault and consistent with the expected and measured fault motion. Although patterns of strain associated with the transition from locked to creeping are not clearly identifiable, a decrease in creep displacement from northwest to southeast along the fault is visible. The observations are in agreement with a model of elastic deformation constrained by *in situ* data that supports a maximum expected deformation signature of 10 mm across the image.

1. Introduction

Parkfield, California is a site of intense study in anticipation of a magnitude 6 earthquake, which according to some predictions appears long overdue [Bakun and Lindh 1985; Roeloffs 1994]. Such an event is expected because magnitude 5.5 to 6 earthquakes apparently ruptured the same segment of the San Andreas fault (SAF) near Parkfield in 1857, 1881, 1901, 1922, 1934, and 1966 [Brown 1967; Sieh 1978; Toppozada 1981], and a slip deficit (total SAF slip minus measured slip) exists that is greater than the coseismic slip that occurred in the last Parkfield earthquake of 1966 [Harris and Segall 1987]. The section of the SAF near Parkfield is the transition zone between the central creeping segment to the northwest and the locked segment to the southeast. The 170 km central segment is creeping aseismically at approximately 32 mm/yr with negligible strain accumulation [Savage 1973; Thatcher 1979]. Slip in the transition zone decreases rapidly to nearly zero southwest of Parkfield, the beginning of the southern locked segment [Lisowski 1981]. Consequently, the southern locked segment accumulates large amounts of strain released in less frequent large to great earthquakes, *e.g.* the magnitude 8 Fort Tejon earthquake of 1857.

Differential radar interferometry [Gabriel et al. 1989; Massonnet et al. 1993] has the unique capability of measuring small deformation signals over wide areas with fine spatial resolution. We have applied the technique using radar data from the European Remote Sensing (ERS-1) satellite to map potential aseismic slip and transitional wide area deformation at Parkfield in this pre-seismic interval. The ERS-1 radar observes the SAF from a direction 23 degrees from vertical at an altitude of roughly 800 km. ERS-1 is in a near polar orbit, so the SAF right-lateral motion of 32 $\mathrm{mm\,a^{-1}}$, for example, would project into a component of displacement in the radar line-of-sight direction of about 10 $\mathrm{mm\,a^{-1}}$. The signal of greatest interest at Parkfield (and at any transition or locked fault segment) is deviations from this secular motion that would indicate transient strain. The magnitude of these signals is expected to be smaller than the secular displacement across the fault, and hence more difficult to decipher and interpret. The interest lies in modeling these deviations to gain insight into possible variations of locking depth, fault geometry and other possible influences that would lead to a better understanding of the Parkfield segment of the SAF.

2. Observations

Several scenes of ERS-1 C-band and SIR-C L-band radar data (see electonic supplement Table 1) were processed from raw signal data to form interferograms [Zebker et al. 1994a; Rosen et al. 1996]. Of these an ERS pair derived from data collected on May 3, 1992 and June 27, 1993 (orbits 4180-10192), with an average baseline of 3 meters and a 420-day temporal interval, was selected for analysis. The correlation of this interferogram was superior to all other processed ERS pairs. Combination of interferogram pairs did not improve the analysis because the SAF regions in the other ERS interferograms were essentially noise. The L-band data had good correlation away from the cultivated regions but the displacement signal could not be seen clearly in the limited swath over the six month observation interval. The interferogram in Figure 1a depicts the phase difference between these favored ERS passes, which is proportional to the combination of the surface displacement measured in the line-of-sight direction and any radar signal propagation differences.

Figure 1

A sharp displacement discontinuity is present through much of the image, similar in character to a creep signature seen along the Garlock fault after the Landers earthquake [Massonnet et al. 1993]. While the Garlock slip is almost certainly coseismic, in this case at Parkfield, the discontinuity may be interpreted as aseismic slip along the SAF. For comparison, Figure 1b shows the active faults within the region [Jennings 1992], overlaid on the image. The line depicting the SAF precisely traces the displacement locus. The largest earthquake to occur in the observation interval was M=5.4 in San Juan Bautista, so none of the signature is coseismic. This is the first time radar interferometry has measured aseismic creep.

Several characteristics of the imagery are of interest. 1) Other apparent signatures appear in the image. These signatures are often associated with mountains or valleys but do not uniformly follow topographic contours. Many of the large fluctuations in phase are presumably due to propagation effects, in this case likely water vapor variability from pass to pass, as has been noted in several recent reports, *e.g.* [Zebker et al. 1997]. Neither these nor the SAF signature can be attributed to topographic artifacts in the processing because the baseline was zero in the center of the image, (ambiguity height of infinity), and therefore had no sensitivity to topography. 2) The slip distribution appears to be non-homogenous along the fault. It is known from surveying (see modelling section for references) that slip at the surface decreases from the northwest to the southeast, at which location the fault becomes locked. The local variability of slip along the fault has not previously been measured, however. The arrows in Figure 1a point to regions where the signature is continuous across the fault. The along-strike profile in Figure 1d clearly shows one of the locations where this occurs. Even in the presence of water vapor errors spanning the fault, a discontinuity in the phase should remain. Several parallel faults have been mapped that may distribute slip over a broader zone. It is not known if the fault was locked at this location during the observation interval. 3) There is a hint that the displacement signature bifurcates in the Northwest quadrant of the image. The Calaveras fault traces precisely the locus of the bifurcated signal.

3. Model Results and Comparison

A model of expected surface deformation constructed for comparison with the differential interferogram is shown in Figure 1c. The distribution of slip was modelled as dislocations in a homogeneous elastic half-space [Okada 1985; Feigl and Dupre *in press*], with constant slip on each of seven fault plane segments, each vertically oriented and slipping in a right lateral sense (see electronic supplement Table 2). The seven fault plane segments were colocated with small-aperture trilateration networks (see Figure 2 from [King et al. 1987]) and slip rates were constrained by data from these networks and from creepmeter measurements [Schulz et al. 1982; Langbein 1997] and GPS measurements (K. J. Hurst, unpublished data, 1997). The slip rate was assumed constant at 32 mm/yr below 16 km depth on all segments and to the surface along the creeping segment off the scene to the northwest. The shallow (16 km to the surface) segment at the southeast corner in the area of Parkfield was locked.

The vector displacement as computed by the Okada model were projected into the radar look direction. The model suggests that the relative slip in the northwest, projected in the radar direction, should be $\approx$10 mm over the 14 month interval. The observations in Fig. 1 are consistent, variously indicating 1/3 of a radar fringe, which corresponds to roughly 10 mm. Equivalently, the envelope of measured slip profile in Fig. 1d, which is scaled to units of right lateral slip, matches the model parameters in Table 2 rather well. To the southeast, the creeping section of the SAF goes through a transition zone to the locked section. The surface deformation pattern changes from a sharp discontinuity to a broad gradient of elastic strain build-up across the SAF. With noisy measurements, it is difficult to detect this long-wavelength feature. A more detailed examination of the strain signature must await improved observations.

4. Conclusions and Discussion

These results show compelling evidence of aseismic slip along the SAF. Though this motion has been well documented through various geodetic measurements, radar observations provide a spatially continuous image of slip, synoptic in time and space, that cannot be obtained by other means, and that may lead to refined models of dynamic fault behavior. Unfortunately, the hit-and-miss observations of ERS or RADARSAT, limited by water vapor-induced displacement errors, and decorrelation over time, are unlikely to provide unequivocal evidence of the subtle transitional signals that could indicate strain accumulation.

Two conditions must be met for a more definitive interferometric analysis at Parkfield. First, interferograms covering the fault over a distance of roughly 300 km surrounding Parkfield are useful to resolve the steady SAF motion from local deformation. In Figure 1a, the fault slip bifurcates and extends beyond the western boundary of the image, and the locked segment likewise starts near the southwest image boundary. Both parts of the fault are unconstrained by these data. Second, many more interferograms with small baselines and long time separations are needed to reduce the water vapor anomolies, as described elsewhere [Zebker et al. 1997]. This interferogram averaging approach will also help the decorrelation problem: most of the ERS data pairs examined were not useful for analysis individually because of decorrelation, but there were not enough pairs to make averaging useful. Since moist soil and associated vegetation are often found at active fault boundaries because of disruption of groundwater flow and fault line valleys in the fractured rock, displacement signal loss from decorrelation is likely to plague C-band sensing of subtle interseismic signals. While longer wavelength radar observations have been shown to better maintain correlation in vegetated regions [Rosen et al. 1996], few such observations exist for Parkfield. Interferometrists interested in interseismic research at faults in central California should proceed with caution and patience.

Acknowledgments. The authors are grateful to E. Chapin for assistance in constructing a mosaicked USGS digital elevation model of the Parkfield area. Discussions with P. Segall, R. Burgmann, and H. Zebker helped relate the observations to the tectonic setting. This work was performed at the Jet Propulsion Laboratory, California Institute of Technology under contract with NASA through the Topography and Surface Change Program. The European Space Agency provided raw SAR data to ESA PI C. Werner. Reviewers K. Feigl and P. Segall were very generous with improvements.

References

Bakun, W. H. and A. G. Lindh, The Parkfield, California earthquake prediction experiment, *Science, 229,* 1985.

Brown, R. D., and J. G. Vedder, Surface tectonic fractures along the San Andreas fault, in the Parkfield-Cholame, California earthquakes June-August 1966, U.S. Geol. Surv. Prof. Pap., *579,* 2-23, 1967.

Feigl, K. L. and E. Dupre, RNGCHN: A program to calculate displacement components from dislocations in an elastic half-space with applications for modeling geodetic measurements of crustal deformation, *Computers and Geosciences, in press.*

Gabriel, A. K., R. M. Goldstein, and H. A. Zebker, Mapping small elevation changes over large areas: differential radar interferometry, J. Geophys. Res., *94,* 9183-9191, 1989.

Harris, R. A., and P. Segall, Detection of a locked zone at depth on the Parkfield, California, segment of the San Andreas fault, J. Geophys. Res., *92,* 7945-7962, 1987.

Jennings, C. W., Preliminary fault activity map of California 1992, *Open File Rep., 92-03,* 76 pp., Calif. Div. of Mines and Geol., Sacramento, 1992.

King, N. E., P. Segall, and W. Prescott, Geodetic measurements near Parkfield, California, 1959-1984, J. Geophys. Res., *92,* 2747-2766, 1987.

Langbein, J., Parkfield creep meter data: detrended measurements from the past 10 years, *http: //quake.wr. usgs.gov /QUAKES/geodetic /twocolor/ creep_pkf_10 yr_det.gif.*

Lisowski, M., and W. H. Prescott, Short-range distance measurements along the San Andreas fault system in central California, 1975 to 1979, Bull. Seismol. Soc. Am., *71,* 1607-1624, 1981.

Massonnet, D., M. Rossi, C. Carmona, F. Adragna, G.Peltzer, K. Feigl, and T. Rabaute, The displacement field of the Landers earthquake mapped by radar interferometry, *Nature, 364,* 138-142, 1993.

Okada, Y., Surface deformation due to shear and tensile faults in a half-space, Bull. Seismol. Soc. Am., *75,* 1135-1154, 1985.

Roeloffs, E., The earthquake prediction experiment at Parkfield, California. Rev. Geophys., *32,* 315-335, 1994.

Rosen, P. A., S. Hensley, H. A. Zebker, F. H. Webb, and E. J. Fielding, Surface deformation and coherence measurements of Kilauea Volcano, Hawaii, from SIR-C radar interferometry, J. Geophys. Res., *101,* 23109-23125, 1996.

Savage, J. C., and R. O. Burford, Geodetic determination of relative plate motion in central California, J. Geophys. Res., *78,* 832-845, 1973.

Schulz, S. S., G. M. Mavko, R. O. Burford, and W. D. Stuart, Long-term fault creep observations in central California, J. Geophys. Res., *87,* 6977-6982, 1982.

Sieh, K. E., Central California foreshocks of the great 1857 earthquake, Bull. Seismol. Soc. Am., *68,* 1731-1749, 1978.

Thatcher, W., Systematic inversion of geodetic data in central California, J. Geophys. Res., *84,* 2283-2297, 1979.

Toppozada, T. R., C. R. Real, and D. L. Parke, Preparation of isoseismal maps and summaries of reported effects for pre-1900 California earthquakes, U.S. Geol. Surv. Open File Rep., *81-11 SAC,* 182 pp., Calif. Div. of Mines and Geol., Sacramento, 1981.

Zebker, H. A., C. L. Werner, P. A. Rosen, and S. Hensley, Accuracy of topographic maps derived from ERS-1 interferometric radar, *IEEE Trans. Geosci. Remote Sens., 32,* 823-836, 1994.

Zebker, H. A., P. A. Rosen, and S. Hensley, Atmospheric effects in interferometric synthetic aperture radar surface deformation and topographic maps, J. Geophys. Res., *102,* 7547-7563, 1997.

P. A. Rosen, C. L. Werner, E. J. Fielding, S. Hensley, Jet Propulsion Laboratory, 4800 Oak Grove Drive, Pasadena, CA, 91109, USA, e-mail: (par@parsar; cw@vega; ericf@kahn; sh@kaitak) .jpl.nasa.gov

S. M. Buckley, The University of Texas at Austin, Center for Space Research, 3925 West Braker Lane, Suite 200, Austin, TX, 78759-5321, USA, e-mail: buckley@csr.utexas.edu

P. Vincent, Campus Box 216, CIRE, University of Colorado at Boulder, Boulder, CO, 80309, USA, e-mail: Paul.Vincent@colorado.edu

(Received August 21, 1997; revised November 28, 1997; accepted January 6, 1998.)

Figure 1. a) ERS-1 differential interferogram showing the relative displacement signature of the aseismic creep distribution near Parkfield, California from May 3, 1992 to June 27, 1993, as projected in the radar line-of-sight direction. One color depicts a displacement of 1.75 mm relative to its neighbor, wrapping in color above 28 mm. Arrows denote areas where phase is continous across the fault. The filled circle below the colorbar denotes the approximate location of zero displacement, in (a-c); b) Same as (a) but with planimetric information (UTM projection), coastlines (blue), and Holocene (green) and historic (orange) faults overlayed. Displacement signature in (a) exactly aligns with the creeping segment of the San Andreas fault. Small squares indicate the location of fault segments used in modeling. White lines across the SAF indicate end points of profile in (d); c) Simulation of aseismic creep along the fault using the slip parameters of Table 2. Projections as in (b). Direction from surface to radar as (east,north,zenith) unit vector is (0.33, −0.08, −0.94); d) Profile along the SAF of relative slip, formed from the difference of profiles (4 km averages normal to fault) taken on either side of the SAF. Extent of profile is indicated in (b).

Figure 1. a) ERS-1 differential interferogram showing the relative displacement signature of the aseismic creep distribution near Parkfield, California from May 3, 1992 to June 27, 1993, as projected in the radar line-of-sight direction. One color depicts a displacement of 1.75 mm relative to its neighbor, wrapping in color above 28 mm. Arrows denote areas where phase is continous across the fault. The filled circle below the colorbar denotes the approximate location of zero displacement, in (a-c); b) Same as (a) but with planimetric information (UTM projection), coastlines (blue), and Holocene (green) and historic (orange) faults overlayed. Displacement signature in (a) exactly aligns with the creeping segment of the San Andreas fault. Small squares indicate the location of fault segments used in modeling. White lines across the SAF indicate end points of profile in (d); c) Simulation of aseismic creep along the fault using the slip parameters of Table 2. Projections as in (b). Direction from surface to radar as (east,north,zenith) unit vector is (0.33, −0.08, −0.94); d) Profile along the SAF of relative slip, formed from the difference of profiles (4 km averages normal to fault) taken on either side of the SAF. Extent of profile is indicated in (b).

5. Electronic Data Supplement

Table 1. Processed Radar Observations

Sensor	Date/ Orbit	Date/ Orbit	[a]B_T (days)	[b]$B_\perp$ (m)
1. ERS-1	1992/07/12 5182	1993/06/27 10192	350	46
2. ERS-1	1992/05/03 4180	1993/06/27 10192	420	-3
3. ERS-1	1992/06/07 4681	1993/09/05 11194	455	115
4. SIR-C	1994/04/13 ...	1994/10/10 ...	180	37

[a] Time Interval (Temporal Baseline)
[b] Mean Perpendicular Baseline Over Entire Image

Table 2. Model Fault Segments for Parkfield Slip

[a]Segment	[b]Easting (m)	[b]Northing (m)	Strike (°)	Length (km)	Width (km)	Depth (km)	[c]Slip (mm)
1[d]	735676	3968326	140.7	9.70	16	16	5.75
2	732287	3972456	140.6	5.34	16	16	11.50
3	725352	3981100	140.3	11.08	16	16	17.25
4	715570	3991980	138.0	14.63	16	16	23.00
5	703281	4004728	136.1	17.71	16	16	28.75
6	687026	4022967	138.3	24.43	16	16	34.50
7	687026	4022967	318.3	1000.00	16	16	37.95
8[e]	735676	3968326	140.7	1000.00	9984	10000	37.95
9	732287	3972456	140.6	5.34	9984	10000	37.95
10	725352	3981100	140.3	11.08	9984	10000	37.95
11	715570	3991980	138.0	14.63	9984	10000	37.95
12	703281	4004728	136.1	17.71	9984	10000	37.95
13	687026	4022967	138.3	24.43	9984	10000	37.95
14	687026	4022967	318.3	1000.00	9984	10000	37.95

[a]Segments are vertically oriented and slipping in a right lateral sense.
[b]Easting and Northing of northwest segment corner.
[c]Slip represents displacement over 14-month period between scenes.
[d]Faults 1-7 are shallow
[e]Faults 8-14 are at depth

ROSEN ET AL.: ASEISMIC CREEP ALONG SAN ANDREAS FAULT

ROSEN ET AL.: ASEISMIC CREEP ALONG SAN ANDREAS FAULT

ROSEN ET AL.: ASEISMIC CREEP ALONG SAN ANDREAS FAULT

ROSEN ET AL.: ASEISMIC CREEP ALONG SAN ANDREAS FAULT

ROSEN ET AL.: ASEISMIC CREEP ALONG SAN ANDREAS FAULT

ROSEN ET AL.: ASEISMIC CREEP ALONG SAN ANDREAS FAULT

ROSEN ET AL.: ASEISMIC CREEP ALONG SAN ANDREAS FAULT

ROSEN ET AL.: ASEISMIC CREEP ALONG SAN ANDREAS FAULT

ROSEN ET AL.: ASEISMIC CREEP ALONG SAN ANDREAS FAULT

ROSEN ET AL.: ASEISMIC CREEP ALONG SAN ANDREAS FAULT

ROSEN ET AL.: ASEISMIC CREEP ALONG SAN ANDREAS FAULT

ROSEN ET AL.: ASEISMIC CREEP ALONG SAN ANDREAS FAULT

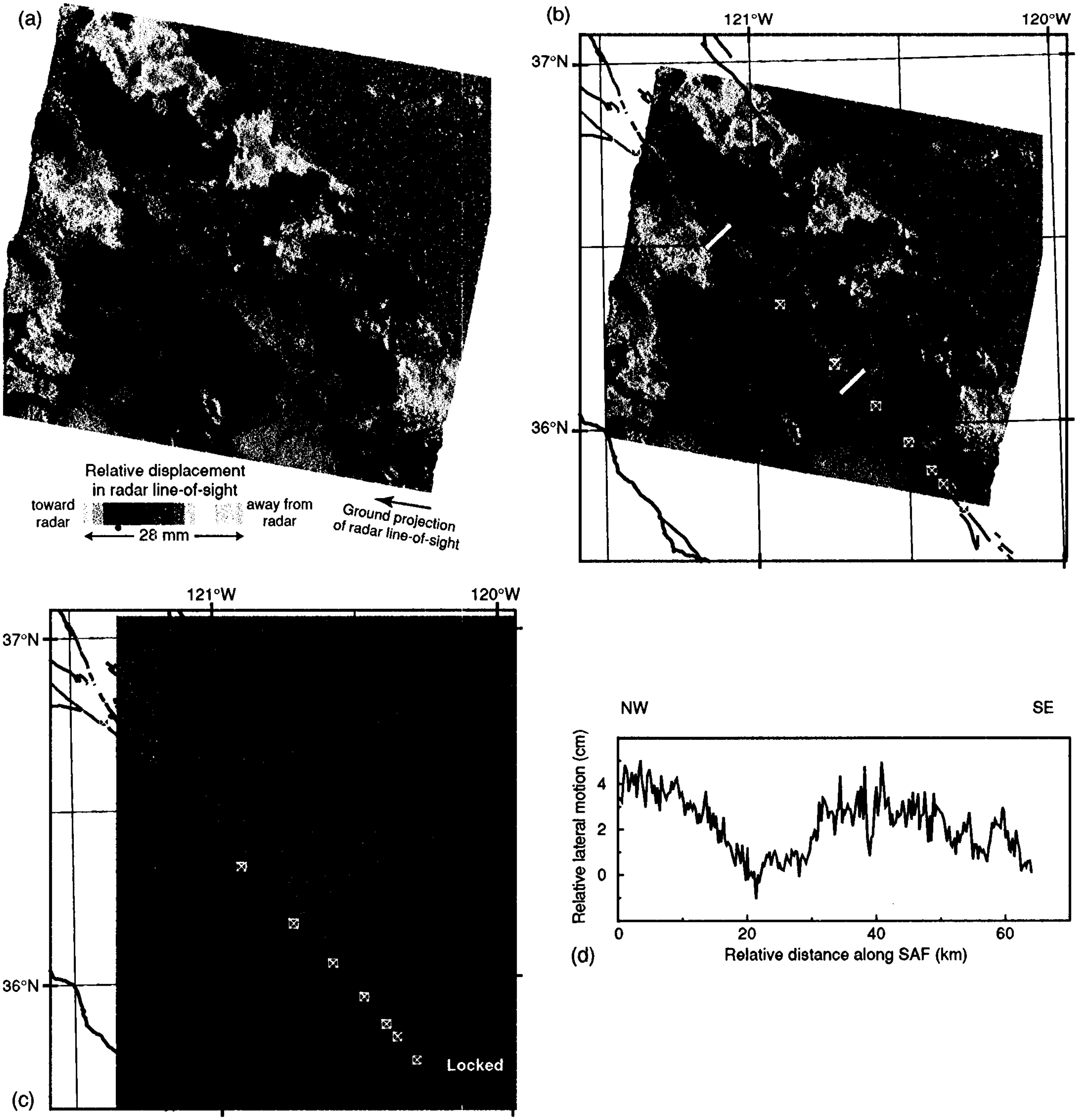
(a)
Relative displacement
in radar line-of-sight
toward
radar
away from
radar
28 mm
Ground projection
of radar line-of-sight
(b)
121°W
120°W
37°N
36°N
(c)
121°W
120°W
37°N
36°N
Locked
NW
SE
Relative lateral motion (cm)
4
2
0
0
20
40
60
Relative distance along SAF (km)
(d)